MODELING AND SIMULATION OF NANOFLUID FOR HEAT STORAGE

by

YATISH NAGARAJ

Presented to the Faculty of the Graduate School of

The University of Texas at Arlington in Partial Fulfillment

of the Requirements

for the Degree of

MASTER OF SCIENCE IN MECHANICAL ENGINEERING

THE UNIVERSITY OF TEXAS AT ARLINGTON

December 2014

To my Mother K Vasantha Nagaraj, Father S C Nagaraj, Sister Mamatha Nagaraj and Brother in law Anand K J, who set an example and motivated me and made me who I am.

ACKNOWLEDGEMENTS

I would like to thank my supervising professor Dr. Alan Bowling for constantly motivating and encouraging me, and also for his invaluable advice during the course of my Master's studies. I wish to thank my academic advisor Dr. Siechii Nomura.

I would also like to extend my gratitude to Dr Donghyun Shin for valuable suggestions. I would also like to thank Dr Adnan Ashfaq for taking time to serve in my thesis defense committee.

I wish to thank my lab mates, Ashley Chase Guy and Anudeep Palanki for their thoughtful suggestions and Mahdi Haghshenas-Jaryani, Adrian Rodriguez for their support.

Finally, I wish to thank my friends Gangadhar Rajashekaraiah, Subhash Seshadri, Aviesh Anand, Thyag Ravi, Snigdha Malladi, Shamali Vardhmane and Apurva Ramavarapu who directly or indirectly helped me complete my thesis and for their constant support during challenging times.

November 24, 2014

ABSTRACT

MODELING AND SIMULATION OF NANOFLUID FOR HEAT STORAGE

Yatish Nagaraj, M.S.

The University of Texas at Arlington, 2014

Supervising Professor: Dr. Alan Bowling

This work models the dynamic behavior of molten nitrate salt mixture to investigate the formation of interfacial nanostructures in ionic liquid nanofluids which is responsible for increase of heat capacity of the mixture. A key application of these fluids is in heat storage in solar collector where the heat capacity determines the amount of energy storage and therefore the efficiency of a solar collector system.

The heat capacity can be significantly increased by the addition of a small amount of nanoparticles, of radius 1 to 100 nanometers in a concentration of $\approx 1\%$ by weight. This increase appears to be caused by the formation of nanostructures in the fluid, initiated by the addition of nanoparticles, is observed by other researchers.

This work is aimed at developing a multi-scale analysis to formulate a simulation that facilitates investigation of the physical phenomena behind nanostructure formation. Finally, the future scope for this work is presented.

TABLE OF CONTENTS

LIST OF ILLUSTRATIONS

CHAPTER 1

INTRODUCTION

Depleting fossil fuels has forced the use of renewable sources of energy for generating electricity. Solar energy is the feasible source as it is available in vast reserves as the sun provides with 120,000 Tera watts of energy per hour [1]. The amount of sunshine in most areas is sufficient to generate around 100-130 GWh of electricity per year from a surface area of 1 km^2. This amount of energy is the equivalent of the annual production of a traditional 50MW power station fueled by coal or natural gas [2]. However, it is a challenge to store this energy during the day in order to generate electricity during the night or under cloudy conditions.

Concentrated Solar Power (CSP) plants, as shown in Figure 1.1 [3], has the technology to store the heat energy and utilize this energy when desired, hence this is a feasible alternative. Countries such as United States, Spain and Germany have considered concentrated solar power as a potential substitute to the non-renewable sources for power generation since the 1980's. These plants use solar energy to heat the heat transfer fluid (HTF) to generate steam which runs the turbines. CSP stores the excess heat in a thermal energy storage (TES) unit when the sun's energy is at the peak and delivers that energy during the later stages of the day when needed [4].

In these plants, solar energy is reflected onto a small area which contains the HTF using mirrors or lens such as the parabolic troughs, Striling Engines or concentrating dishes or power tower system as shown in the figure. The heat collected in the HTF is transferred to a boiler or a TES [5]. The most commonly used HTF are the mineral oils, however these oils decompose at high temperatures. Since CSP plants

employ conventional thermodynamic cycles (e.g., Rankine cycle, Brayton gas turbine cycle, etc.) to produce electricity similar to other conventional energy systems, it is desired to operate at high temperatures to enhance energy conversion efficiency. Hence the mineral oils are replaced with molten salt due to its ability to achieve higher temperatures [6].

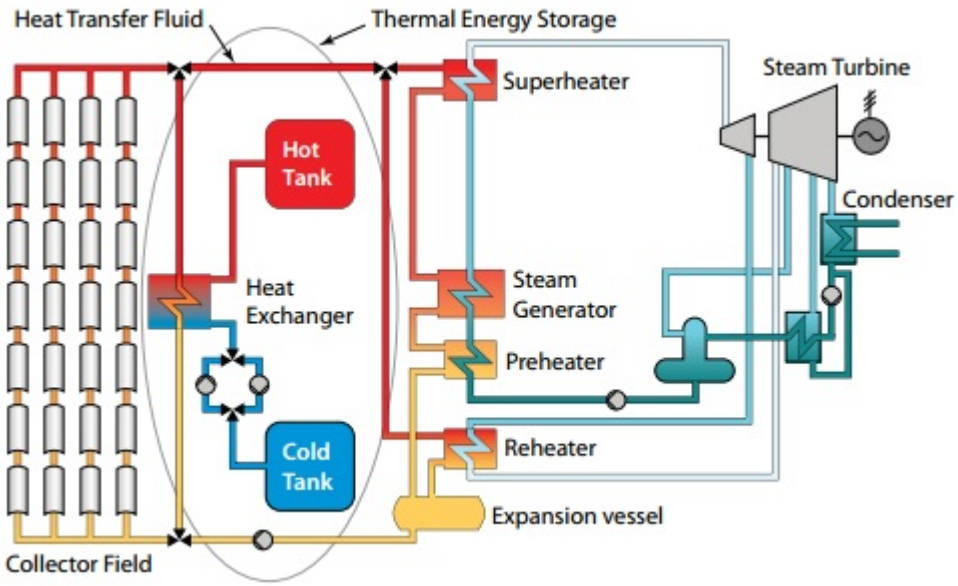

Figure 1.1. Schematic of Concentrated Solar Power Plant.

The specific heat of the storage material in the TES needs to be higher than the HTF for better efficiency. Conventional TES fluids are not thermally stable at high temperatures due to their low evaporation point or thermal decomposition. The critical point of water is only 374.14 ^oC at 221.2 bar and organic TES fluids, such as oil and ethylene glycol, decompose well below 400 ^oC. Hence many researches are making an effort to increase the specific heat capacity of molten salts using oxide nanoparticles [7][8][9]. This composite mixture is called *ionic liquid nanofluid* which is a suitable material for TES.

In addition, the cost to construct / maintain a CSP operating with a high temperature HTF and TES is considerable. Costs associated with the HTF/TES fluid are approximately 25% of the total CSP plant operating costs. A key way to reduce these costs is to improve the heat capacity of the facilities (storage tanks) and transport structures (pipe and heat exchanger systems). According to a recent cost analysis by Excelergy, 30% increase of heat capacity can reduce the cost approximately 19%, which is equivalent to $11 million saving on TES capital cost without changing material and operational costs, see Figure 1.2 [10].

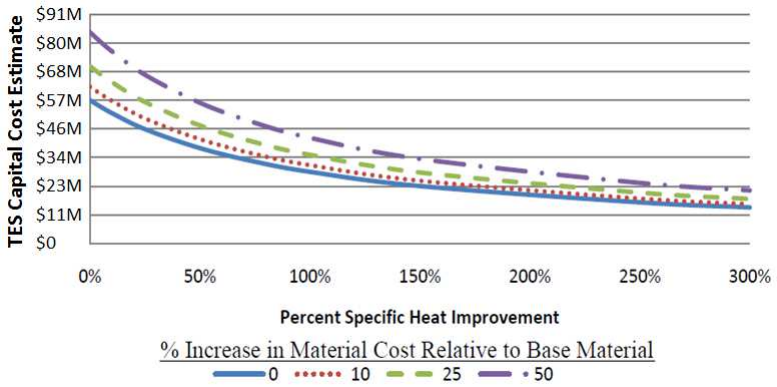

Figure 1.2. TES capital cost predicted by NREL Excelergy model.

A mixture of $NaNO_3$ and KNO_3 is currently used as a TES in the mostly recently build CSP plants [11]. The specific heat capacity of this mixture is increased upto 28% with the addition of SiO_2 nanoparticles [12]. This increase in heat capacity is due to the nanostructures formed by the addition of the nanoparticles.

The goal of this thesis is to study the proposed mechanism for enhanced specific heat capacity. Understand the mechanism of nanostructure formation and provide the first generation model of ionic liquid nanofluid. Also to address the possible multiscale issues associated with the model.

CHAPTER 2

BACKGROUND

2.1 Experimental Setup

Extremely clean environment is maintained to prevent contamination as discussed in [12]. The preparation of nano-engineered molten salts are to be meticulously carried out to prevent agglomeration. The mixture of $NaNO_3$ and KNO_3 salts must be a homogeneous mixture. The pure material was first studied to get familiar with the structure of the pure nitrate eutectic. When an eutectic of two or more salts are mixed and the material characterization is to be carried out, it is mandatory to able to distinguish the materials mixed in the eutectic. Hence, the Backscattered (BSD) imaging lens were used to distinguish the different materials using different contrast for each salt in the mixture. The material characterization was carried out using the Scanning Electron Microscope (SEM; ZEISS Supra 55 VP) to study the structure of the material. A Modulated Differential Scanning Calorimeter (MDSC) was employed to measure the specific heat capacity.

In order to mix the nitrate eutectic with the silica nanoparticles, a meticulous approach was carried out to get a homogeneous mixture. The method followed to fabricate the base material has three steps: mixing, sonication and dehydration. During mixing, sodium nitrate 60% by weight, potassium nitrate 40% by weight and silica nanoparticles 1% by weight are added manually into the sample. A total of 198 mg of molten salt with 2 mg of silica nanoparticles were mixed in a sample to be tested. 20 ml of distilled water is used as a solvent to mix the salts efficiently. To disperse the nanoparticles inside the mixture and to avoid agglomeration of the

particles at nano scale sonication is carried out. An ultrasonicator is used to sonicate the mixture for approximately 200 minutes in order to ensure excellent dispersion of nanoparticles inside the mixture. The mixture is then dehydrated by placing it on a hot plate at 200^o C for 7 hours. The obtained dehydrated salt is then tested in the MDSC.

The Modulated Differential Scanning Calorimeter (MDSC; Q20, TA Instruments Inc.) was used to measure the specific heat capacity of the salt sample. A total of $15 - 25$ mg of salt sample is loaded on to a pan which is heat for approximately 30 minutes to remove the moisture. The moisture in the sample or in the pan will yield bad results. Hence the pan is sealed to avoid moisture from entering the sample. MDSC basically works on the principle of comparing the thermal energy of two sample simultaneously. One sample being the reference which is empty and the other is the salt loaded sample. The heat flow which is recorded is the reference thermal energy input minus the sample thermal energy input to create a single value which represents the difference in energy required to raise the temperature of the sample and reference items by the same quantity.

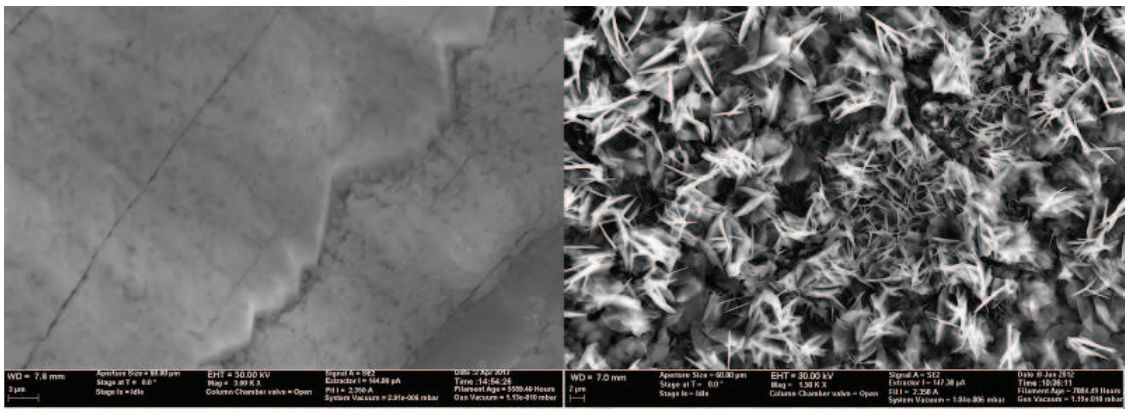

Figure 2.1. Microscopic image of pure sample and sample with nanoparticles.

The specific heat of the samples with nanoparticles increased by upto 28%. When the nanomaterials were put to test under the microscope it was observed that there were strange structures at the microscale at most parts of the sample. This small structures resemble particles, threads or webs at the size of $10 - 100$ nm. This special structures were present only in the salt samples with nanoparticles as shown in the Figure 2.1 [7]. These structures are formed due to the electrostatic interactions between oxidized nanoparticles and ionic liquids [13].

2.2 Molecular Dynamics

Molecular Dynamics is the science of simulating the motions of a system of particles [14]. Molecular Dynamic Simulations (MDS) is a computational method for examining the time variant characteristics of a system on a molecular or atomic scale. These simulations are often used to examine biological phenomena such as the folding of biopolymers. This approach involves modeling every atom in the system and all of the interactions between them. This often leads to simulating high frequency vibrations occurring at the atomic level. A small time step is required to capture the behavior of these systems and thus the time required to obtain a small amount of simulation is large. The figure 2.1 shows the schematic of the nanostructure formation mechanism.

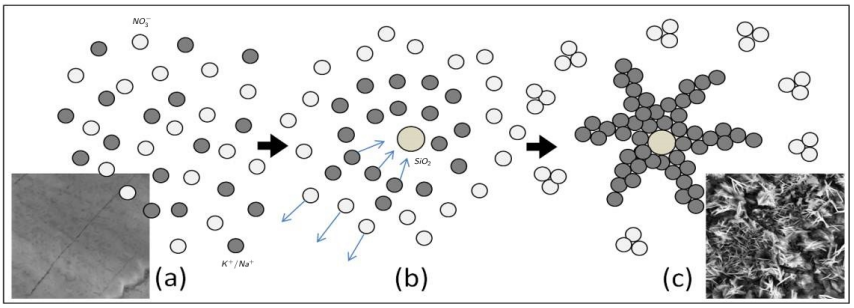

Figure 2.2. Formation of nanostructures around the nanoparticle.

The high frequency vibrations can be eliminated using a process called coarse-graining, which can take several forms [15][16][17][18][19][20][21]. Several approaches have been developed to minimize and speed up the calculations in the coarse-grained model using advances in algorithms [22], as well as improvements in computational hardware and parallel computing [23]and in computational hardware such as graphical processing unit [24]. Coarse-graining of the nanofluid yields a model where large bodies, the nanoparticle interact with small bodies, the ions yielding what is reffered to as a multiscale model. A characteristic of multiscale model is a disproportionality between the size of different terms that yields large accelerations that nust be numerically integrated using a small time step. This disproportionality implies the existence of slow dyynamics as well as fast dynamics. Several analytical techniques have been used to remove the fast dynamics and retain slow dynamics, which allows for larger numerical integration time steps and shorter run times that yield a longer time history of events. These methods include modal analysis which retains only low frequency modes, the small mass assumption which omits the mass terms and leads to the overdamped Langevin model.

Applying the MMS to the nanofluid yields a singular perturbation problem, which is difficult to address using the MMS. The most common alternate approach is to use the small mass assumption, which yields a first order model, the overdamped Langevin equations, that predicts overdamped motion of the system. Several researchers argued that this behavior is physically correct for small particles. However, we argued that this approach produced a model that can violate Newton's second law. A new multiscale analysis model is developed that can address singular pertubation problems that retains the mass properties, yielding a second order model that predicts underdamped motion of small particles in a fluid environment characterized by a low Reynolds number. These methods can be used to reduced the simulation

run time and also increase the number of bodies in the system, which will allow the formation of nanostructures.

CHAPTER 3

METHOD IMPLEMENTED

3.1 Rigid Multibody Model

A system with sodium ions, potassium ions and all the atoms in SiO_2 nanoparticles can be modeled as a nanofluid. However, this results in a model with high degrees of freedom; also large number of atoms bound up in the nanoparticle will vibrate at high frequencies, which requires a small time step that drastically increases the simulation run time. Course-graining is a technique to represent a system by a reduced number of degrees of freedom. Hence, the nanoparticle is modeled as a single rigid body, assuming the atoms in the nanoparticle do not move relative to each other and are lumped together. Thus reducing the number of bodies and degrees of freedom, which eliminates the high frequency vibrations between the atoms within the nanoparticle and reduces the simulation run time. This process is known as $coarse - graining$. The inertia terms are retained in the rigid body based model in order to remain true to the original molecular dynamic model [21].

Fig. 3.1 represents a 2D coarse grained mechanical model which is not drawn to scale. This model represents SiO_2 nanoparticle, Na^+ ions, K^+ ions and NO_3^- ions. The following assumptions are made in order to meet the objectives of this study.

Assumptions

1. The effect of inter-atomic vibrations in the nanoparticle are ignored.
2. The nanoparticle develops a uniform surface negative charge as it is exposed to water.
3. The nanoparticle along with sodium, potassium and nitrate ions are rigid spheres.

The mechanical model is comprised of rigid bodies inside a boundary to conserve the total mass of the system as shown in the Fig. 3.1. The system contains one nanoparticle along with 50% by number of $NaNO_3$ and 50% of KNO_3. The mass centers of each body are represented by small half filled circles. Since the nitrogen and oxygen in NO_3^- are rigidly bound, the collection is modeled as a single rigid sphere with a net charge of -1.

The vectors $\hat{N}_1$ and $\hat{N}_2$ in Fig. 3.1 define the inertial reference frame. All other reference frames are attached to the different bodies. In the molten state, the crystalline lattice structure of the nitrate salt breaks down into its component ions, Na^+, K^+ and NO_3^- and are free to move throughout the volume. However, at the operating temperature the nanoparticle remains a rigid solid sphere. To represent the system lets consider one $NaNO_3$, one KNO_3 and one SiO_2 nanoparticle. The first NO_3^- ion has three degrees of freedom denoted by q_1, q_2 and q_3. The angular rotation is about the $\hat{N}_3$ direction ($= \hat{N}_1$ x $\hat{N}_2$) is represented by q_3. The second NO_3^- ion has three degrees of freedom denoted by q_4, q_5 and q_6. The angular rotation is about the $\hat{N}_3$ direction ($= \hat{N}_1$ x $\hat{N}_2$) is represented by q_6. Na^+ ion has 3 degrees of freedom denoted by q_7, q_8 and q_9. The angular rotation is about the $\hat{N}_3$ direction ($= \hat{N}_1$ x $\hat{N}_2$) is represented by q_9. K^+ ion has 3 degrees of freedom denoted by q_{10}, q_{11} and q_{12}. The angular rotation is about the $\hat{N}_3$ direction ($= \hat{N}_1$ x $\hat{N}_2$) is represented by q_{12}. SiO_2 nanoparticle has 3 degrees of freedom denoted by q_{13}, q_{14} and q_{15}. The angular rotation is about the $\hat{N}_3$ direction ($= \hat{N}_1$ x $\hat{N}_2$) is represented by q_{15}.

Consider a system with s and n degrees-of-freedom to describe the position and orientation of the ions and nanoparticle respectively, the total degrees of freedom of the system $N = s + n$.

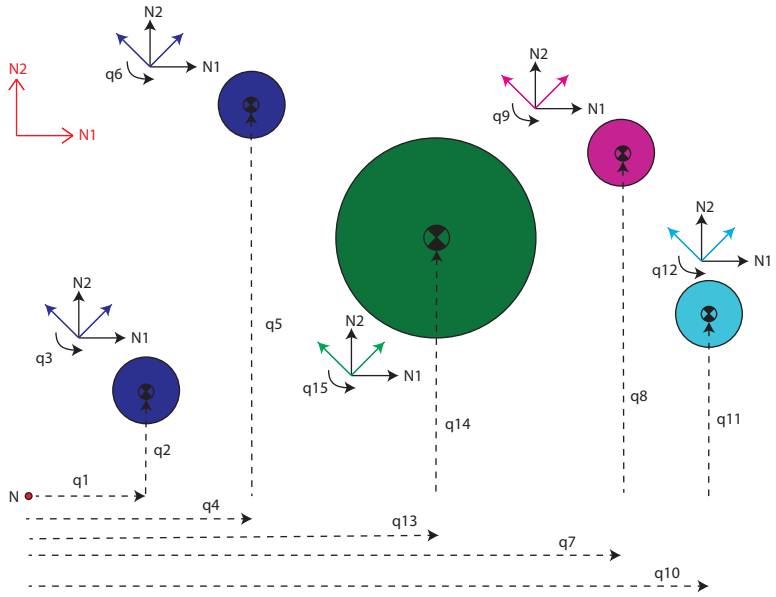

Figure 3.1. Mechanical System.

The multibody mechanical model have the form:

$$\begin{bmatrix} m & 0 \\ 0 & M \end{bmatrix} \begin{bmatrix} \ddot{q}_m \\ \ddot{q}_M \end{bmatrix} = A\ddot{q} = \mathbf{\Gamma} \tag{3.1}$$

where the mass matrix $A \in \mathbb{R}^{N\times N}$ includes $m \in \mathbb{R}^{s\times s}$ and $M \in \mathbb{R}^{n\times n}$, $\mathbf{q} = [q_m \;\; q_M]^T$ are the generalized coordinates, $\dot{\mathbf{q}} = [\dot{q}_m \;\; \dot{q}_M]^T$ and $\ddot{\mathbf{q}} = [\ddot{q}_m \;\; \ddot{q}_M]^T$ are the generalized speeds and accelerations, and $\mathbf{\Gamma}$ contains the generalized active forces. While the terms on the left represent the generalized inertia forces.

The generalized active forces includes the forces due to viscous friction, charge potentials, the Nosé-Hoover thermostat, containment and Brownian motion as shown below.

$$\mathbf{\Gamma} \;=\; \begin{bmatrix} \mathbf{\Gamma}_m \\ \mathbf{\Gamma}_M \end{bmatrix} \;=\; \begin{bmatrix} 0 \\ \mathbf{\Gamma}_{friction} \end{bmatrix} + \mathbf{\Gamma}_{potential} + \mathbf{\Gamma}_{thermostat} + \mathbf{\Gamma}_{containment} + \mathbf{\Gamma}_{brownian} \tag{3.2}$$

where $\mathbf{\Gamma}_{friction} \in \mathbb{R}^{n\times 1}$, $\mathbf{\Gamma}_{potential} \in \mathbb{R}^{N\times 1}$, $\mathbf{\Gamma}_{thermostat} \in \mathbb{R}^{N\times 1}$, $\mathbf{\Gamma}_{containment} \in \mathbb{R}^{N\times 1}$ and $\mathbf{\Gamma}_{brownian} \in \mathbb{R}^{N\times 1}$.

The Knudsen number for the ions is too large to satisfy a continuum assumption, so viscous friction is not applied to ions, but only to the nanoparticle. The viscous friction acting on the nanoparticle is represented by the following expression:

$$\mathbf{\Gamma}_{friction} = -D\dot{q}_M \tag{3.3}$$

where $D \in \mathbb{R}^{n\times n}$ is a diagonal matrix containing the translational and rotational drag coefficients; which transforms the frictional forces and moments applied at the mass center of the nanoparticle into generalized active forces. These forces are discussed in detail in the following sections.

The unit of mass, the *Zeptogram (zg)* is chosen so that the mass values of the nitrate is in the order 10^{-1}, and the length and time units, the *Nanometers (nm)* and *Nanoseconds (ns)* are chosen for similar reasons. The masses and inertias are contained in the mass matrix A in Eq.3.1, which is symmetric, positive definite and a diagonal matrix.

3.2 Mass and Inertia Calculation

Mass of bodies

The mass of sodium and potassium ions is calculated based on the individual molar masses of the ions. The mass of the nitrate ion is calculated based on the atomic masses in the molecule. The nitrate ion contains, $1-Nitrogen$ and $3-Oxygen$ atoms and hence the atomic weight is 62.0049 $gmol^{-1}$ ($1 \times 14.0049 + 3 \times 16$). The mass of one nitrate ion is 0.10296 zg, which is got by dividing the atomic weight of nitrate with the number of molecules in one mole of a given substance i.e. the Avagadro's

number ($N_A = 6.022 \times 10^{23}\ mol^{-1}$). The mass of the other ions are calculated in a similar manner (refer Appendix A)

The mass of the nanoparticle is calculated based on the density and volume of the nanoparticle. The density of SiO_2 is 2.648 g/cm^3 [25]. The rest of the calculation is shown in Appendix A.

Inertia of bodies

The inertia of all the bodies are based on the following assumptions.

Assumptions:

1. Each body is assumed to be a rigid sphere.
2. The radius of each sphere is assumed to be the effective packing radii of monovalent ions [26].

The inertias are calculated about the mass center of each body in the $\hat{N}_3$ axis direction. The detailed calculation of the inertias is in Appendix B.

3.3 Frictional Forces

The following assumptions are made for simplicity in calculating the drag forces on this system:

Assumptions

1. The fluid is assumed to be Newtonian fluid with uniform viscosity at 773K.
2. Each atom is assumed to be a solid sphere and the effective radii of atoms is used for the radius of sphere.

For calculating the viscous forces, the system falls in the transition region between the Statistical and Continuum mechanics formulation of fluid dynamics. A dimensionless Knudsen number (K_n) can be used to classify which formulation could be used.

Knudsen number is defined as the ratio of the molecular mean free path length to a representative physical length. If the Knudsen number is near or greater than one, the mean free path of a molecule is comparable to a length scale of the problem, and the continuum assumption of fluid mechanics is no longer a good approximation.

$$K_n = \frac{\gamma}{L} \tag{3.4}$$

where γ is the mean free path of the the fluid and L is the length scale. The Knudsen number is too large for the ions so the continuum assumption is no longer a good approximation, whereas the Stoke's Law can be used to calculate viscous forces for the nanoparticle.

The linear drag coefficient (β) and rotational drag coefficient (β_w) for a sphere is given by

$$\beta = 6\pi\mu r \tag{3.5}$$

$$\beta_w = 8\pi\mu r^3 \tag{3.6}$$

where, μ is the viscosity of the medium and r is the radius of the sphere.

3.4 Potential Forces

The structures are formed due to the charge potentials between the Na^+ ions, K^+ ions and the SiO_2 nanoparticle. The potential energy is modeled as pair potential which includes Coulomb potential and Lennard-Jones potential. The following assumptions are made in order to obtain the structures.

Assumptions

1. The nanoparticle develops surface negative charge due to the presence of OH^- in the solution [7].
2. Sodium and potassium ions are point charges.

Coulomb Potential

The Coulomb potential (Φ_C) is an effective pair potential that describes the interaction between two point charges, is given by the expression shown in Eq.3.4 [27]

$$\Phi_C = \frac{q_i q_j}{4\pi\epsilon_0\epsilon_r r_{ij}} \tag{3.7}$$

where Φ_C is the Coulomb Potential; q_i, q_j are the Coulomb Charges; ϵ_0 is the Permittivity of vacuum; ϵ_r is the Relative Permittivity and r_{ij} is the Distance between the charges.

Lennard-Jones Potential

The Lennard-Jones Potential (Φ_{LJ}) is a simple model which approximates the interaction between a pair of atoms or molecules. It consists of an attractive and a repulsive term, as the atoms cannot overlap in space. The Lennard-Jones potential for a pair is given relations shown below [28]:

$$\Phi_{LJ} = 4\epsilon_{ij}\left[\left(\frac{\sigma_{ij}}{r_{ij}}\right)^{12} - \left(\frac{\sigma_{ij}}{r_{ij}}\right)^{6}\right] \tag{3.8}$$

$$\epsilon_{ij} = \sqrt{\epsilon_i \epsilon_j} \tag{3.9}$$

$$\sigma_{ij} = \frac{\sigma_i + \sigma_j}{2} \tag{3.10}$$

where, Φ_{LJ} is the Lennard-Jones Potential; ϵ_i, ϵ_j is the minimum value of potential for particle i and particle j; σ_i, σ_j is the finite distance at which the inter-particle potential is zero for particle i and particle j; and r_{ij} is the distance between the particles.

Total Interaction Potential

The total interaction potential (Φ) is the sum of Coulomb Potential and Lennard-Jones Potential.

$$\Phi(r) = \Phi_C + \Phi_{LJ} = \frac{q_i q_j}{4\pi\epsilon_0\epsilon_r r_{ij}} + 4\epsilon_{ij}\left[\left(\frac{\sigma_{ij}}{r_{ij}}\right)^{12} - \left(\frac{\sigma_{ij}}{r_{ij}}\right)^{6}\right] \tag{3.11}$$

The net potential forces can be calculated by taking the derivative of total potential energy ($\Phi(r)$) with respect to the distance (r) as shown below:

$$\Gamma_{potential} = \frac{d\Phi(r)}{dr} \tag{3.12}$$

$$\Gamma_{potential} = -\frac{q_i q_j}{4\pi\epsilon_0\epsilon_r r_{ij}^2} + 24\epsilon_{ij}\left(\frac{\sigma_{ij}^6}{r_{ij}^7} - \frac{2\sigma_{ij}^{12}}{r_{ij}^{13}}\right) \tag{3.13}$$

Further information regarding potential parameters and constants is discussed in Appendix C.

3.5 Thermostat Forces

The Nosé-Hoover thermostat is used to maintain the average temperature of the system at a desired value[29]. The temperature control is essential as the structures are formed only when the system is heated to a desired temperature. The Nosé-Hoover thermostat provides the most realistic temperature profiles, ergodic behavior and reliable heat capacities for finite systems [30] [31]. The temperature is maintained by introducing a new term using the following equations [32]:

$$\frac{d\zeta}{dt} = \left(\frac{1}{2}\dot{q}^T A\dot{q} - \frac{1}{2}Nk_B T_d\right)\frac{2}{Q} \tag{3.14}$$

$$\Gamma_{thermostat} = -\zeta A\dot{q} \tag{3.15}$$

where, ζ represents the flow of thermal energy into or out of the system, k_B is the Boltzmann constant, T_d is the desired temperature of the system, Q is the gain used to adjust the rate of thermal energy flow. This thermostat can add and remove energy from the system, taking a form similar to friction which is a function of the momentum of each body and serves as a feedback mechanism to control the temperature, depending on the value of ζ. The time derivative of ζ is determined by the difference between the kinetic energy and its average.

The response to the change in temperature can be controlled using the thermostat gain, Q, in order to maintain the average temperature of the system. A lower value of Q has a quicker response to the change in temperature and a higher value of Q has a slower response to the change in temperature.

3.6 Containment Forces

The containment forces are added to conserve the mass of the system. The containment forces are modeled as hard sphere repulsion potentials. The boundary is modeled as imaginary hard sphere at a specific radius R, and the ions are modeled with radius equal to the effective packing radius, r_e. If the ions get closer to the boundary, then the ions repel like hard spheres as shown in the figure. This repulsive force is numerically modeled using the following expression:

$$\Phi_r = \frac{B}{r^6} \tag{3.16}$$

where, Φ_r is the containment potential, B is a constant, r is the distance between the boundary and the ion. The containment forces can be calculated by taking the derivative of the above expression with respect to the distance r as shown below:

$$\Gamma_{containment} = \frac{d\Phi_r}{dr} \tag{3.17}$$

$$\Gamma_{containment} = \frac{-6B}{r^7} \tag{3.18}$$

3.7 Brownian Forces

The Brownian motion is added to the system to represent the collisions between a modeled body and an unmodeled body. The Brownian motion for this study is modeled from the already established method of modeling Brownian motion on Motor proteins and optical tweezers [33] [34].

Random forces and moments in the model, representing Brownian motion, are implemented as Gaussian white noise. They act at the center of mass for each body in the system and is expressed as the following,

$$f_{Bo} = B_{o1}(t)\hat{N}_1 + B_{o2}(t)\hat{N}_2 \tag{3.19}$$

Where, $B_{o1}(t)$ and $B_{o1}(t)$ represents the forces produced by randomly fluctuating thermal noise applied in the $\hat{N}_1$ and $\hat{N}_2$ direction respectively. Each component of the random force and moment is treated independently as a normally distributed random variable. They have the following *expectations*, $E[.]$, or weighted average values:

$$E[B_{oi}(t)] = \langle B_{oi}(t) \rangle = 0 = \mu \tag{3.20}$$

and are governed by a fluctuation-dissipation relation expressed as

$$E[B_{oi}(t_1)B_{oj}(t_2)] = 2\beta k_B T \delta(t_1 - t_2)\delta_{i,j} \tag{3.21}$$

where k_B and T are the Boltzmann constant and absolute temperature, respectively. The relation in 3.12 implies that there is no time dependency between the random processes over time; the random sequence of forces does not repeat regularly. In addition 3.12 and 3.13 imply

$$E[B_{oi}^2(t)] = 2\beta k_B T = Var(B_{oi}(t)) = \sigma^2 \tag{3.22}$$

which is the variance of B_{oi}. Thus, B_{oi} can be generated using an Eigen function $gsl_rng_set(gsl_rng, rand())$ which generates random variables with a normal distribution.

The collection of random forces comprise $\Gamma_{brownian}$. Theses randomly fluctuating discontinuous functions show numerical integration and so each random variables is held constant during a single integration step; the random variables i updated at the

beginning of each step. Thus, the value of each random variable is known before the integration step, and the decomposed value of the random force must equal it. This is accomplished by defining

$$\Gamma_{brownian} = R_{nd} r_{nd} = R_{nd} \begin{bmatrix} B_{o1} \\ B_{o2} \\ B_{o3} \\ . \\ . \end{bmatrix} \tag{3.23}$$

where, R_{nd} transforms the random forces into generalized active forces. See Appendix E for further details about modeling the Brownian motion.

3.8 Multiscale Analysis

One of the problems that occur for modeling the micro and nano scale systems is the disproportionality between the mass and the forces acting on them. This disproportionality would cause large accelerations which can only be captured with small time steps. This increases the simulation run time to possibly days to months. One of the methods to address this disproportionality is by using proper scaling factors to scale the forces, so that they cancel each other out while retaining the dynamics of the system, therby reducing the simulation run time [35]. Since this model involves small masses, one of the key aspects of this paper is to address the possible multiscale nature of the system. The modified equations of motion with the scaling factor (a_2) is:

$$\begin{bmatrix} m & 0 \\ 0 & M \end{bmatrix} \begin{bmatrix} \ddot{q}_m \\ \ddot{q}_M \end{bmatrix} = \mathbf{\Gamma}_{thermostat} + a_2 \left(\begin{bmatrix} 0 \\ \mathbf{\Gamma}_{friction} \end{bmatrix} + \mathbf{\Gamma}_{potential} + \mathbf{\Gamma}_{containment} + \mathbf{\Gamma}_{brownian} \right) \tag{3.24}$$

Refer to Appendix F for the derivation of the above expression.

CHAPTER 4

RESULTS AND DISCUSSION

Results

The plots shown in Figure 4.1 and 4.2 are the initial positions and the final positions of all bodies in the unscaled system. The plots in Figure 4.5 and 4.6 are the initial and final positions of all the bodies in the scaled system. The pink circle represents the nanoparticle (30nm diameter), the red circle represents the sodium ions and the green circle represents the potassium ions where as the small points represents the nitrate ions. The temperature profiles are shown in the Figure 4.3, 4.4, 4.5 and 4.6.

The simulation in Figure 4.1 has 100 bodies and the temperature was being maintained at 525K with the thermostat gain (Q) of 40. It is noticed the sodium and potassium ions move towards the nanoparticle forming the nanostructures, where as the nitrate ions move away from the nanoparticle. The average temperature of the system is maintained at 525K depicted by the red line in the Figure 4.3. The initial temperature is high as the system is not in the equilibrium state, as the simulation continues the system reaches its equilibrium state and temperature fluctuation reduces. The total simulation time for 0.2ns time history was 21 days.

A similar behavior of the nanofluid as shown in Figure 4.2 is observed when the number of bodies are increased to 200. The results remain consistent with the previous result, the nanostructures are formed due to the sodium and potassium ions. The average temperature of the system was also maintained at the desired temperature.

Numerous simulations with varying bodies and temperatures (upto 773K) provided similar results for the unscaled system.

The simulation in Figure 4.5 has 100 bodies and the temperature was being maintained at 575K with the thermostat gain (Q) of 40 with a scaling factor of 0.4. It is noticed the sodium and potassium ions move towards the nanoparticle forming the nanostructures, where as the nitrate ions move away from the nanoparticle, this behavior is identical to the unscaled system. The average temperature of the system is maintained at 575K depicted by the red line in the Figure 4.7. The total simulation time for 0.5ns time history was 12 days, which is 77% reduction in simulation time compared to the unscaled system. The simulation results with a scaling factor of 0.5 is show in Figure 4.6 and the respective temperature profile in Figure 4.7.

The simulations with a lower scaling factor below 0.4 reduced the simulation run time, however the nanostructure formation was not noticed. This could be due to the non-linearity of the potential force equations. Which can be addressed to in the future.

Discussion

By comparing the simulation of the unscaled system in Figure 4.1. with the simulations of the scaled system in Figure 4.5 and Figure 4.6, it is evident the initial positions of all the bodies are the same however the final positions are different since the trajectory of the particles in the scale system is different. The actual behavior of the system is unclear as the system is of very low scale, however the density of the simulated system can be compared to the density of the physical system. This can be done by increasing the number of bodies in the simulated system.

In the equation 3.24 of the scaled system, the value of a_2 is a greater than or equal to the value of ϵ (Appendix F) which is the fraction of the mass of the body and the potential constants. As the mass of the ions is of the order $\mathcal{O}(-1)$, where

as the mass of the nanoparticle is of the order $\mathcal{O}(4)$. This difference in the scale of the masses of different bodies could limit the value of the scaling factor to 0.4. This could be addressed by scaling the forces on the ions alone, by retaining the unscaled equations for the nanoparticle as shown below, this can reduce the simulation run time further:

$$\begin{bmatrix} m & 0 \\ 0 & M \end{bmatrix} \begin{bmatrix} \ddot{q}_m \\ \ddot{q}_M \end{bmatrix} = \mathbf{\Gamma} \tag{4.1}$$

where,

$$\mathbf{\Gamma} = \begin{bmatrix} \mathbf{\Gamma}_m \\ \mathbf{\Gamma}_M \end{bmatrix} = \begin{bmatrix} \mathbf{\Gamma}_{thermostat} + a_2(\mathbf{\Gamma}_{potential} + \mathbf{\Gamma}_{containment} + \mathbf{\Gamma}_{Brownian}) \\ \mathbf{\Gamma}_{thermostat} + \mathbf{\Gamma}_{frictional} + \mathbf{\Gamma}_{potential} + \mathbf{\Gamma}_{containment} + \mathbf{\Gamma}_{Brownian} \end{bmatrix} \tag{4.2}$$

Also since the nanoparticle is coarse-grained a lot of energy to maintain the temperature of the system has to be given to the nanoparticle which contains large number of atoms to form the nanocluster, which again can be done by scaling the equation 3.14, this can be addressed to in the future.

Future Scope

Following improvements needs to be made to this work:

1. Three dimensional model of the ionic nanofluid needs to be modeled.
2. The scaling factor needs to be reduced.
3. Increase the number of bodies and calculate the specific heat capacity of the nanofluid.
4. Viscous parameters needs to be validated with literature.
5. Change the circular boundary to a rectangular boundary to satisfy the periodic boundary condition assumption.

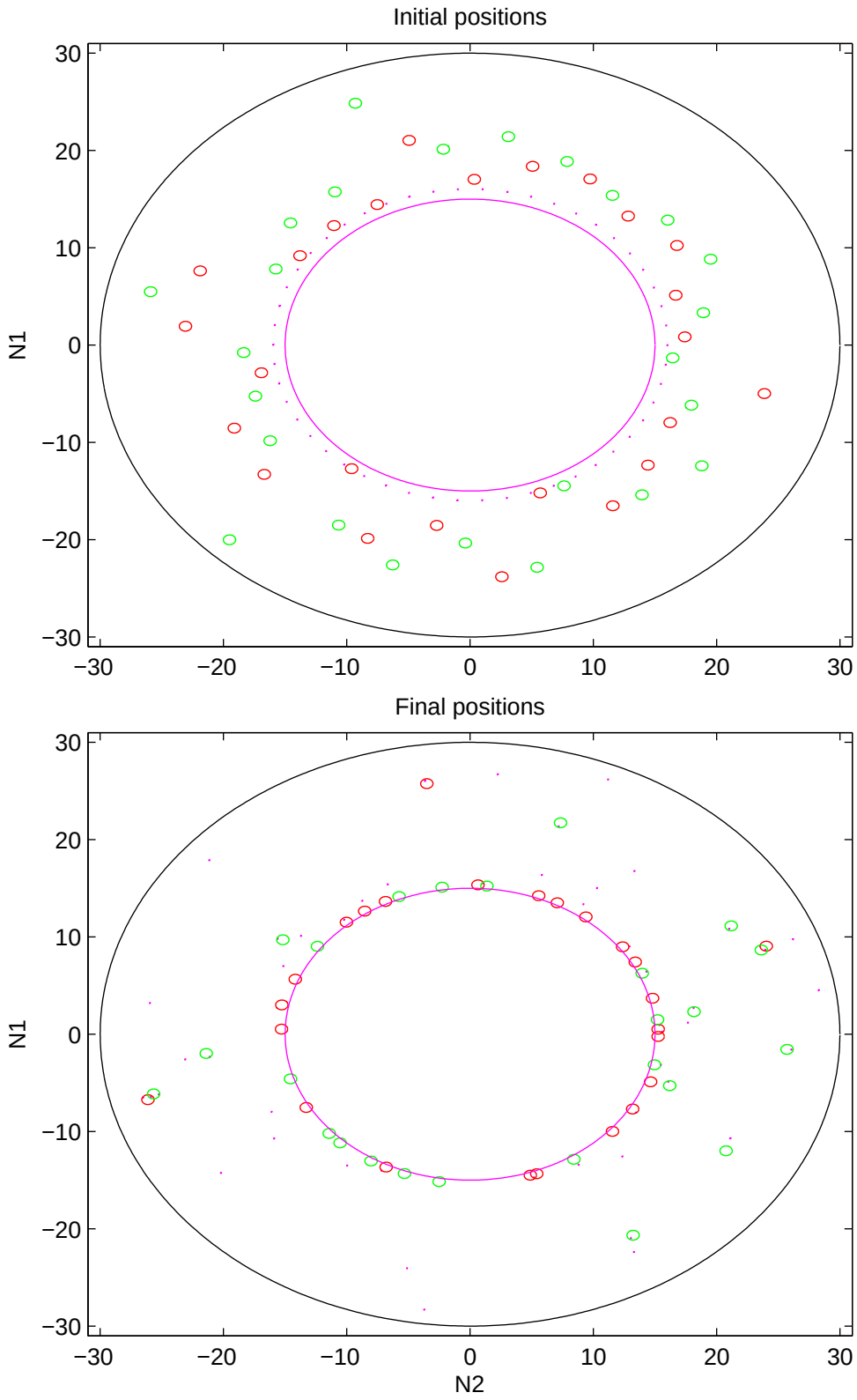

Figure 4.1. Positions of the unscaled system with 100 bodies.

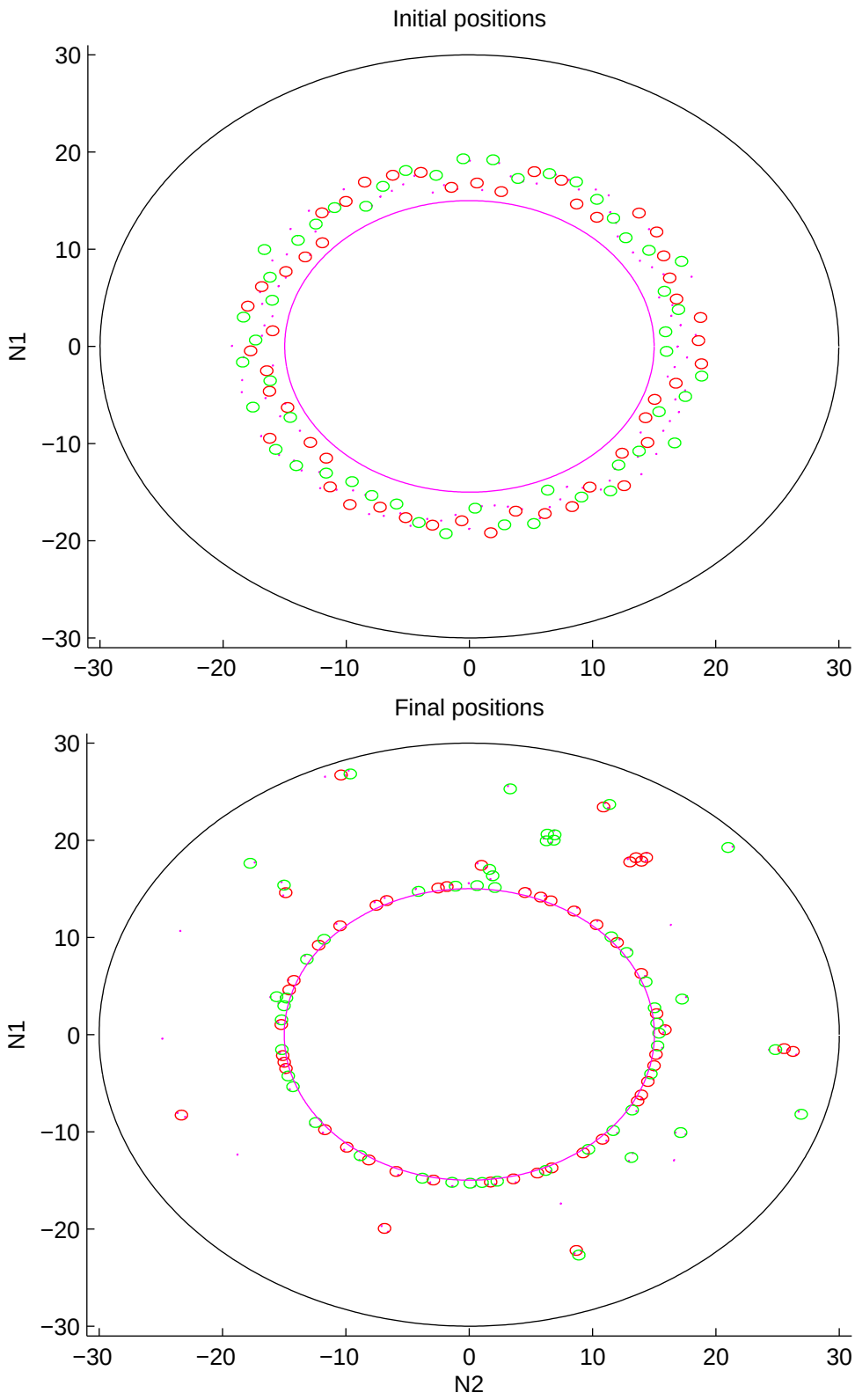

Figure 4.2. Positions of the unscaled system with 200 bodies.

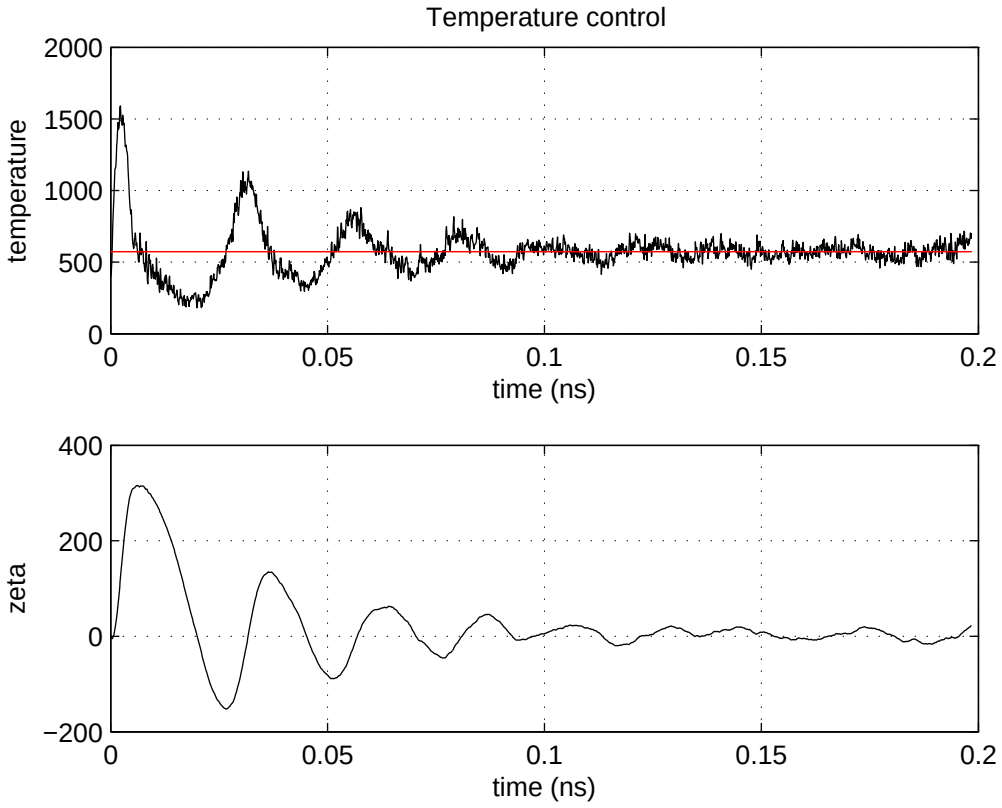

Figure 4.3. Temperature Profile with Q = 40.

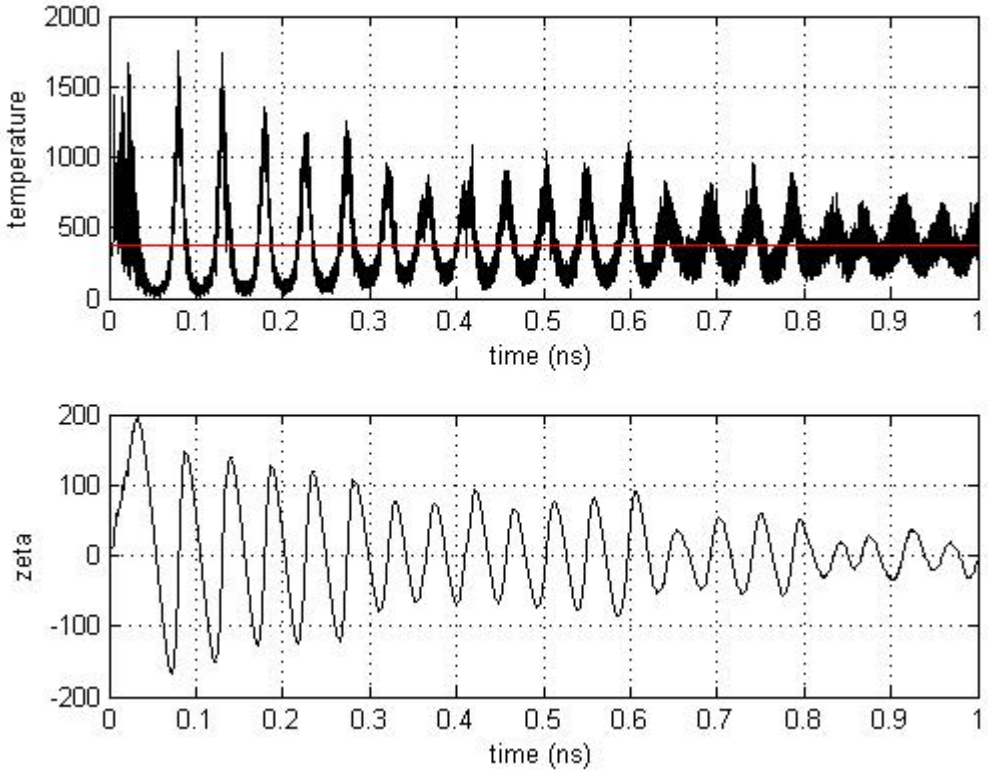

Figure 4.4. Temperature Profile with Q = 30.

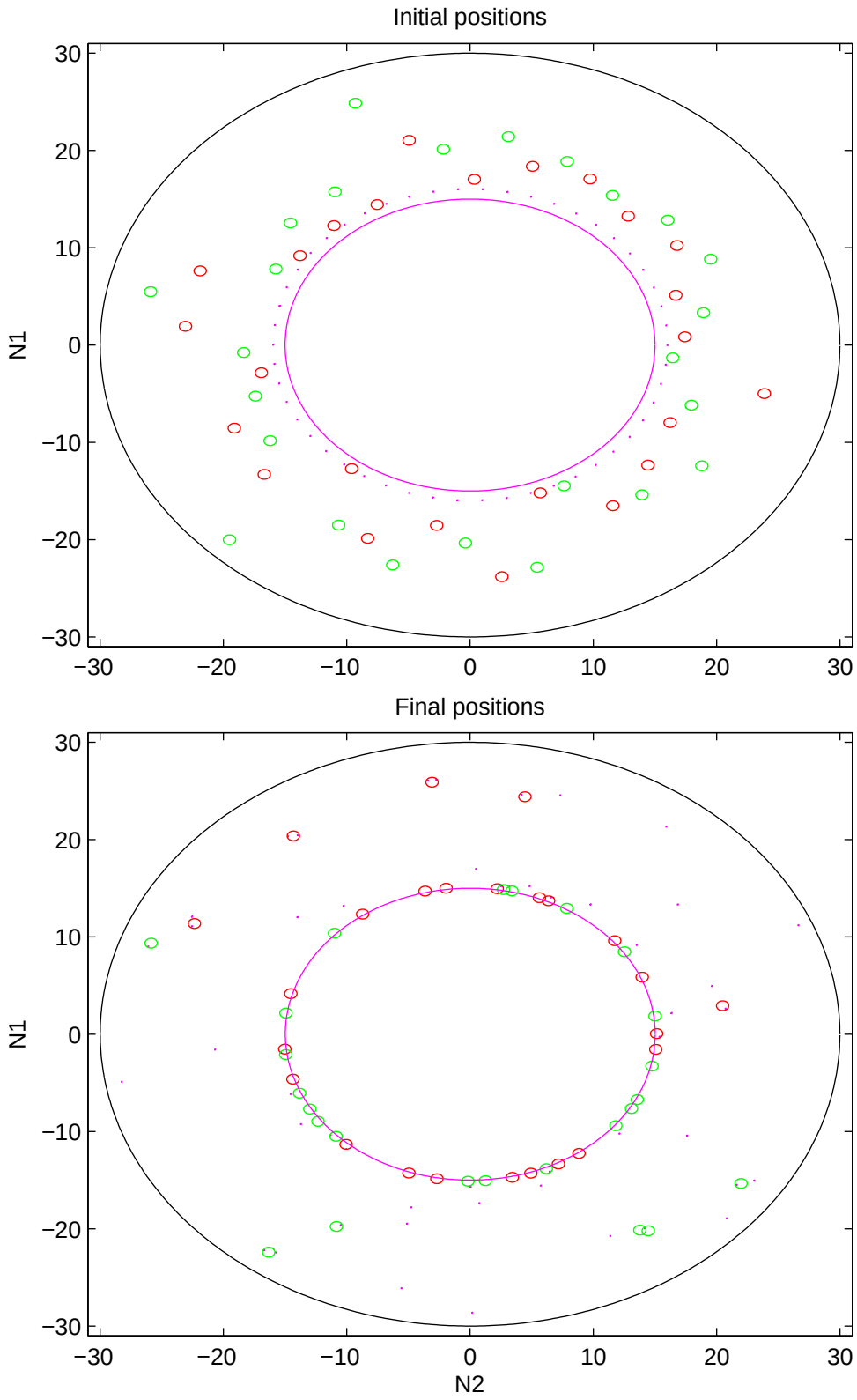

Figure 4.5. Positions of 100 bodies in scaled system with scaling factor of 0.4.

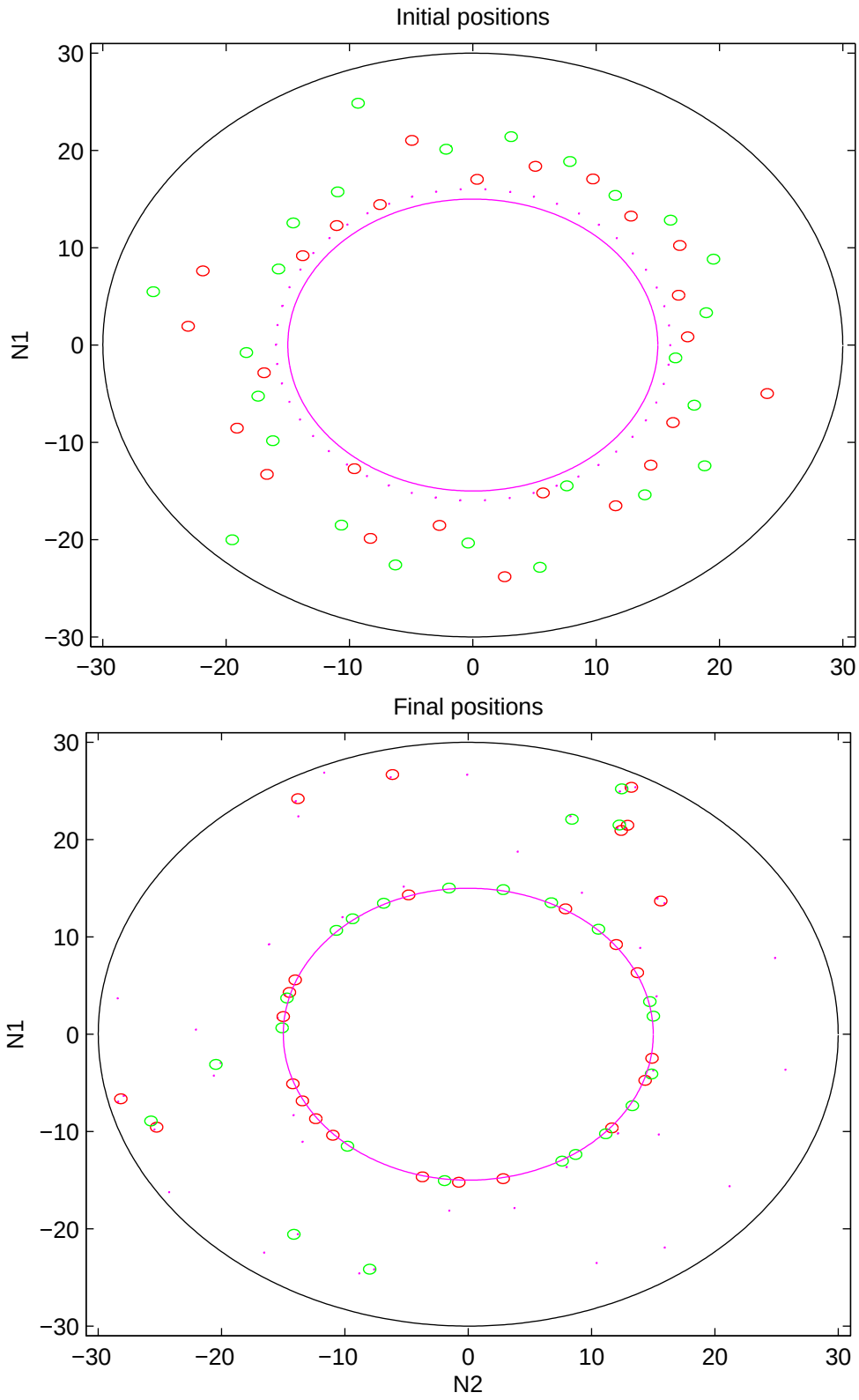

Figure 4.6. Positions of 100 bodies in scaled system with scaling factor of 0.5.

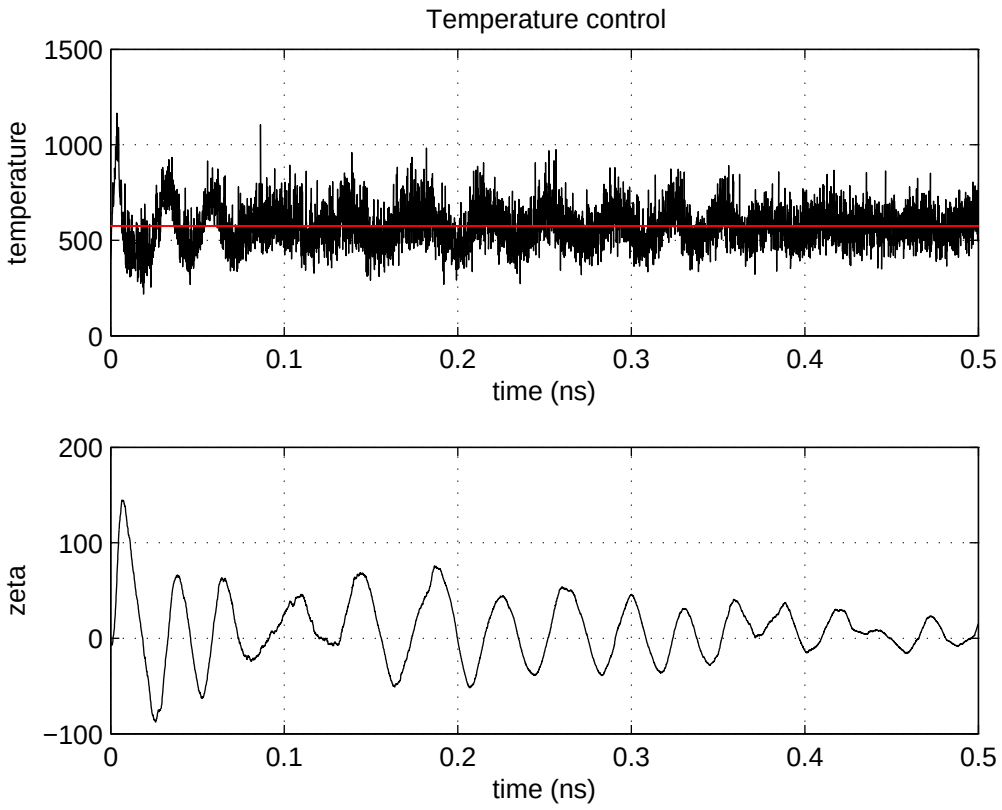

Figure 4.7. Temperature Profile for scaled system with scaling factor of 0.4.

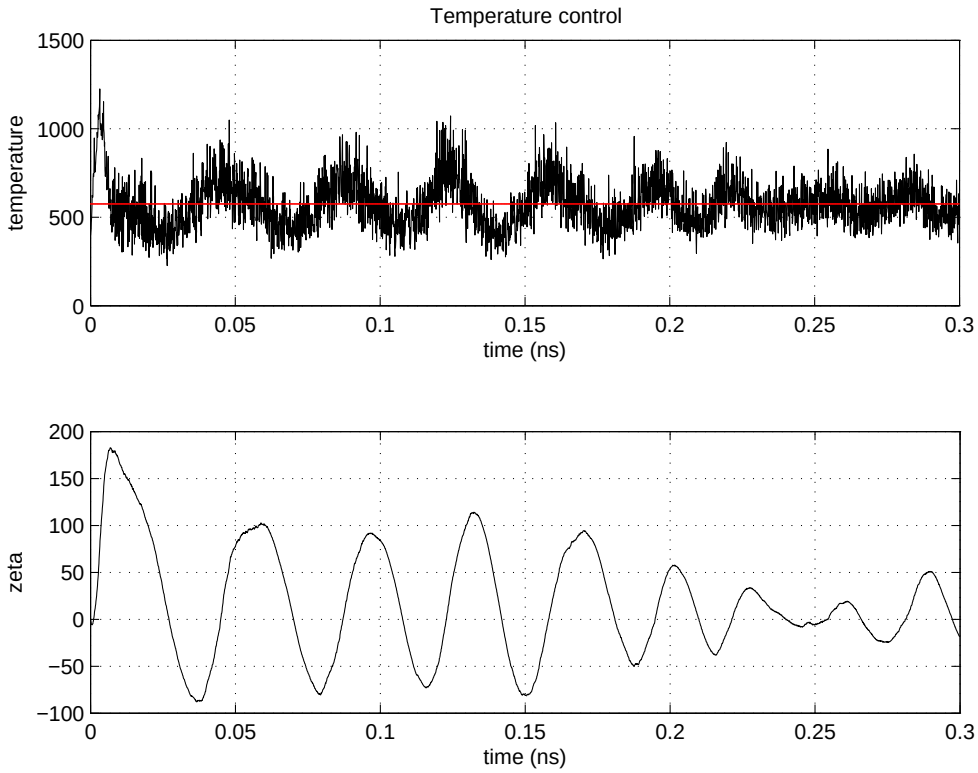

Figure 4.8. Temperature Profile for scaled system with scaling factor of 0.5.

CHAPTER 5

CONCLUSION

The first generation model of the ionic liquid nanofluid is represented. The SiO_2 nanoparticle is coarse-grained and a rigid body model is presented. The various forces acting on the system are described and modeled with proper assumptions. The simulations showing the dynamics behavior of the nanofluid shows the formation of nanostructures. The method of multi-scale was implemented to reduce the simulation run time, which also forms the nanostructures. The temperature of the system is maintained at any desired temperature as shown. Finally, the future scope for this work is presented laying the foundation for a new theoretical approach.

APPENDIX A

Mass Calculations

Mass of Sodium Ions

The molar mass of sodium is 22.99 $gmol^{-1}$. The mass of one sodium ion is got my dividing its molar mass with the Avogadro's number ($N_A = 6.022 \times 10^{23}\ mol^{-1}$). Therefore the mass of one ion of sodium is 0.0381757 zg.

Mass of Potassium Ions

The molar mass of potassium is 39.098 $gmol^{-1}$. The mass of one potassium ion is got my dividing its molar mass with the Avogadro's number ($N_A = 6.022 \times 10^{23}\ mol^{-1}$). Therefore the mass of one ion of potassium is 0.0649237 zg.

Mass of SiO_2 Nanoparticle

Density of $SiO_2 = 2.648\ g\ cm^{-3} = 2.648\ zg\ nm^{-3}$.

Volume of a sphere = $\frac{4}{3}\pi r^3$.

Therefore, volume of 30 nm SiO_2 nanoparticle = $\frac{4}{3}\pi 15^3 = 14137.1669\ nm^3$.

Hence the mass of 30 nm SiO_2 nanoparticle = Density × Volume = 2.648×14137.1669

Therefore the mass of 30 nm SiO_2 nanoparticle is 37435.218 zg

The table below shows the mass of all the bodies.

Ion / Nanoparticle	Mass(zg)
Na^+	0.0381757
K^+	0.0649237
NO_3^-	0.10296
SiO_2	37435.218

Table A.1. Masses of ions and nanoparticle

APPENDIX B

Inertia Calculations

Inertia Calculations: The inertia of all the bodies is based on the following assumptions.

Assumptions

1. Each body is assumed to be a rigid sphere.
2. The effective packing radii of monovalent ions are used as radius of the spheres.

The inertia of the bodies is calculated about the $\hat{N}_3$ axis. For a solid sphere, the inertia (I_{33}) about the $\hat{N}_3$ axis is given by,

$$I_{33} = \frac{2}{5}mr^2 \tag{B.1}$$

where, m is the mass of the ion or nanoparticle; r is the effective packing radii.
The table below lists the effective packing radii for all the bodies.

Ion / Nanoparticle	Radii(nm)
Na^+	0.095
K^+	0.133
NO_3^-	0.264
SiO_2	0.162

Table B.1. Effective packing radii [27][36]

Inertia of Sodium Ions

$$I_{33Na^+} = \frac{2}{5}mr^2 \tag{B.2}$$

$$I_{33Na^+} = \frac{2}{5}(0.0381757)(0.095)^2$$

$$I_{33Na^+} = 0.0001378146 \ \ zg - nm^2$$

Inertia of Potassium Ions

$$I_{33K^+} = \frac{2}{5}mr^2 \tag{B.3}$$

$$I_{33K^+} = \frac{2}{5}(0.0649237)(0.133)^2$$

$$I_{33K^+} = 0.000459374 \ \ zg - nm^2$$

Inertia of Nitrate Ions

$$I_{33NO_3^-} = \frac{2}{5}mr^2 \tag{B.4}$$

$$I_{33NO_3^-} = \frac{2}{5}(0.10296)(0.264)^2$$

$$I_{33NO_3^-} = 0.0028704 \ \ zg - nm^2$$

Inertia of SiO_2 Nanoparticle

$$I_{33SiO_2} = \frac{2}{5}mr^2 \tag{B.5}$$

$$I_{33SiO_2} = \frac{2}{5}(37435.218)(0.162)^2$$

$$I_{33SiO_2} = 392.29799 \ \ zg - nm^2$$

The table below shows the inertia of all the bodies.

Ion / Nanoparticle	Inertia($zg - nm^2$)
Na^+	0.0001378146
K^+	0.000459374
NO_3^-	0.0028704
SiO_2	392.29799

Table B.2. Inertia of ions and nanoparticle

APPENDIX C

Potential Forces

Potential Parameters

The net charge for the nitrate ion is -e it is modeled based on the nitrate structure as shown below [37]. The bond length between N^+ and O^- in the nitrate ion is 0.132 nm [27].

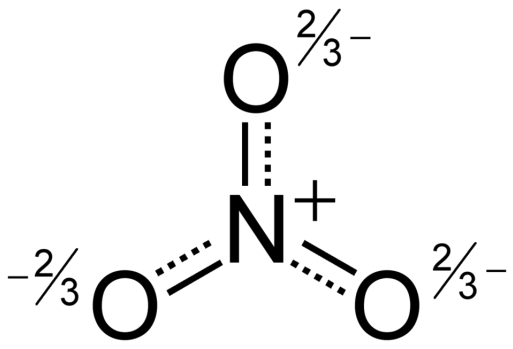

Figure C.1. Nitrate ion Structure.

The potential energy parameters for the individual ions is given in the following table:

Ion / Nanoparticle	Charge(e)	ϵ_r	$\sigma_i/\sigma_j(nm)$	$\epsilon_i/\epsilon_j(zg - nm^2 - ns^{-2})$
Na^+	+1	5.1	0.273	597.794
K^+	+1	5.1	0.30469	694.105
N^+	+1	5.1	0.39	1389.87
O^-	−0.667	5.1	0.3154	1077.69
SiO_2	−1.35	5.1	0.349	1486.46

Table C.1. Potential parameters of ions and nanoparticle[28] [38] [39]

APPENDIX D

Drag Forces

The drag coefficients used for each body are given below:

Ion / Nanoparticle	β	β_w
NO_3^-	4669	433.8
SiO_2	56568.158	707424.21

Table D.1. Drag coefficients

The viscous friction is added only to the nanoparticle, however the Brownian motion acting on the other ions were calculated based on the above values.

APPENDIX E

Brownian Motion

Brownian Motion

For calculating the Brownian motion, the value of β for the below equation is obtained from the Table C.1.

$$E[B_{oi}^2(t)] = 2\beta k_B T = Var(B_{oi}(t)) = \sigma^2 \tag{E.1}$$

The values of k_B and T used in this model is 13.806488 $zg - nm^2(ns^2K)^{-1}$ and $393K$ respectively. The Brownian motion is applied on individual atoms. The Fig. E.1 shows the order of Brownian force calculated for NO_3^-, Na^+ and K^+. The Fig. E.2 shows the order of Brownian force calculated for SiO_2 nanoparticle.

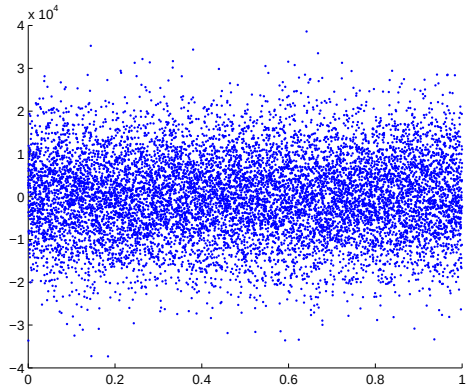

Figure E.1. Brownian Motion acting on ions.

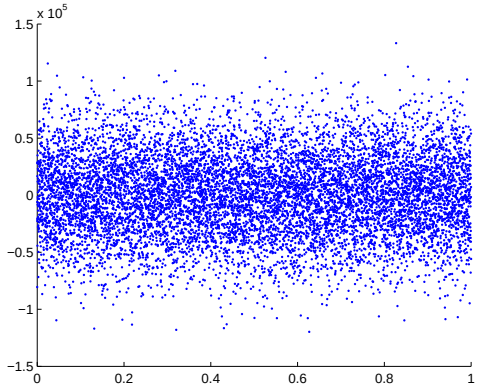

Figure E.2. Brownian Motion acting on nanoparticle.

APPENDIX F

Multiscale Analysis

The Newton-Euler equation for the system is:

$$m\ddot{q} = \Gamma_{viscous} + \Gamma_{potential} + \Gamma_{thermostat} + \Gamma_{containment} + \Gamma_{Brownian} \tag{F.1}$$

As the potential forces are the dominating forces, we group all the other forces in Γ_{others}.

$$m\ddot{q} = \Gamma_{potential} + \Gamma_{thermostat} + \Gamma_{others} \tag{F.2}$$

Expanding potential forces into the Coulomb and the Lennard Jones potential. (Refer to the equation 3.13)

$$m\ddot{q} = \frac{C_1}{r^2} + \frac{C_2}{r^7} + \frac{C_3}{r^{13}} - \zeta m\dot{q} + \Gamma_{others} \tag{F.3}$$

where, C_1, C_2, C_3 are the constants for the coulomb potential, Lennard Jones attraction and repulsion potential respectively. The values of these constants vary depending on the interacting pair of ions. (Refer Appendix C)
Dividing the equation with either of these constants say C_1,

$$\frac{m\ddot{q}}{C_1} = \frac{1}{r^2} - \frac{\zeta m\dot{q}}{C_1} + \frac{\Gamma_{others}}{C_1} \tag{F.4}$$

The value of $\frac{m}{C_1} \approx 2.3 \times 10^{-4}$ which is small, yielding a large acceleration that is difficult to numerically integrate. Assuming $\frac{m}{C_1} = \epsilon$, the value of ϵ varies from 10^{-4} to 10^{-1} depending the interacting atoms and the mass of each body considered.

$$\epsilon\ddot{q} + \epsilon\zeta\dot{q} = \frac{1}{r^2} + \frac{\Gamma_{others}}{C_1} \tag{F.5}$$

The small parameter ϵ is used to decompose time into different scales, $T_i = \epsilon^i t$ yielding:

$$\dot{x} = \frac{dx}{dt} = \epsilon^0 \frac{\partial x}{\partial T_0} + \epsilon^1 \frac{\partial x}{\partial T_1} + \epsilon^2 \frac{\partial x}{\partial T_2} + ... \tag{F.6}$$

$$\ddot{x} = \frac{d^2x}{dt^2} = \sum_{i=0}^{\infty}\sum_{j=0}^{\infty} \epsilon^i \epsilon^j \frac{\partial^2 x}{\partial T_i \partial T_j} \tag{F.7}$$

For the expression F.5 to be true some of the forces on the right must cancel each other. Introducing two constants a_1 and a_2 such that,

$$\epsilon\ddot{q} + \epsilon\zeta\dot{q} = (a_1 + a_2)\left(\frac{1}{r^2} + \frac{\Gamma_{others}}{C_1}\right) \tag{F.8}$$

where, $a_1 + a_2 = 1$. Since some forces must cancel

$$a_1\left(\frac{1}{r^2} + \frac{\Gamma_{others}}{C_1}\right) = 0 \tag{F.9}$$

Therefore,

$$\epsilon\ddot{q} + \epsilon\zeta\dot{q} = a_2\left(\frac{1}{r^2} + \frac{\Gamma_{others}}{C_1}\right) \tag{F.10}$$

Rewriting in the original form,

$$m\ddot{q} = \Gamma_{thermostat} + a_2\left(\Gamma_{viscous} + \Gamma_{potential} + \Gamma_{containment} + \Gamma_{brownian}\right) \tag{F.11}$$

where a_2 has a value greater than or equal to ϵ

BIBLIOGRAPHY

[1] P.E. Glaser, "Power from the sun: Its future," *Science*, vol. 162, pp. 857-861, 1968.

[2] F. Cavallaro, "Fuzzy topsis approach for assessing thermal-energy storage in concentrated solar power (csp) systems," *Applied Energy*, vol. 87, no2, pp. 496-503, 2010.

[3] "Concentrated solar power plants," http://www.nrel.gov/csp/, accessed on : 16th of November, 2014.

[4] V. Quaschning and M. B. Muriel, "Solar power-photovoltaics or solar thermal power plants?" *VGB POWERTECH-INTERNATIONAL EDITION,* vol. 82, pp. 48-52, 2002.

[5] B. Kelly and D. Kearney, "Thermal storage commercial plant design study for a 2-tank indirect molten salt system," 2006.

[6] D. Shin and D. Banerjee, "Enhancement of specific heat capacity of high-temperature silica-nanofluids synthesized in alkali chloride salt eutectics for solar thermal-energy storage applications," *International journal of heat and mass transfer,* vol. 54, no. 5, pp. 1064-1070, 2011.

[7] H. Tiznobaik and D. Shin, "Enhanced specific heat capacity of high-temerature molten salt-based nanofluids," *International Journal of Heat and Mass Transfer,* vol. 57, no. 2, pp. 542-548, 2013.

[8] D. Shin and D. Banerjee, "Enhancement of specific heat capacity of high-temperature silica-nanofluids synthesized in alkali chloride salt eutectics for solar thermal-energy storage applications," *International Journal of Heat and Mass Transfer,* vol. 54, pp. 1064-1070, December 2010.

[9] N. J. Bridges, A. E. Visser, and E. B. Fox, "Potential of nanoparticle-enhanced ionic liquids (neils) as advanced heat-transfer fluids," *Energy Fuels,* col. 25, pp. 4862-4864, September 2011.

[10] D. R. MALIK, "Evaluation of composite alumina nanoparticle and nitrate eutectic materials for use in concentrating solar power plants," Ph.D. dissertation, Texas A&M University, 2010.

[11] R. I. Dunn, P. J. Hearps, and M. N. Wright, "MOlten-salt power towers: newly commercial concentrating solar storage," *Proceeding of the IEEE,* vol. 100, no. 2, pp. 504-515, 2012.

[12] B. Dudda and D. Shin, "Effect of nanoparticle dispersion on specific heat capacity of a binary nitrate salt eutectic for concentrated solar power applications," *International Journal of Thermal Sciences,* vol. 69, pp. 37-42, April 2013.

[13] H. Tiznobaik and D. Shin, "Experimental validation of enhanced heat capacity of ionic liquid-based nanomaterial," *Applied Physics Letter,* vol. 102, no. 17, p. 173906, 2013.

[14] M. Karphus, G. A. Petsko, *et al.,* "Molecular dynamics simulations in biology," *Nature,* vol. 347, no. 6294, pp. 631-639, 1990.

[15] G. Stratopoulos, T. Dialynas, and G. Tsironis, "Directional newtonian motion and reversals of molecular motors," *Physics Letters A,* vol. 252, no. 3, pp. 151-156, 1999.

[16] A. Bowling and A. F. Palmer, "The small mass assumption applied to the multibody dynamics of motor proteins," *Journal of biomechanics,* vol. 42, no. 9, pp. 1218-1233, 2009.

[17] A. D. Schuyler and G. S. Chirikjian, "Nomal mode analysis of proteins: a comparison of rigid cluster modes with coarse graining," *Journal of Molecular Graphics and Modelling,* vol. 22, no. 3, pp. 183-193, 2004.

[18] A. D. Schuyler and G. S. Chirikjian, "Efficient determination of low-frequency normal modes of large protein structures by cluster-nma," *Journal of Molecular Graphics and Modelling,* vol. 24, no. 1, pp. 46-58, 2005.

[19] J. L. Mateos, "Walking on ratchets with two brownian motors," *Fluctuation and Noise Letters,* vol. 4, no. 01, pp. L161-L170, 2004.

[20] M. Poursina and K. S. Anderson, "Long-range force and moment calculations in multiresolution simulations of molecular systems," *Journal of Computational Physics,* vol. 231, no. 21, pp. 7237-7254, 2012.

[21] M. Poursina and K. S. Anderson, "Canonical ensemble simulation of biopolymers using a coarse-grained articulated generalized divide-and-conquer scheme," *Computer Physics Communications,* vol. 184, no. 3, pp. 652-660, 2013.

[22] S. N. Medyanik and W. K. Liu, "Multiple time scale method for atomistic simulations," *Computational Mechanics,* vol. 42, no. 4, pp. 596-577, 2008.

[23] K. Anderson, M, Poursina and K. Bhalerao, "On adaptive multiscale modeling of biomolecular system with application in rna," in *Proceeding of the Joint International Conference on Multibody System Dynamics,* 2010.

[24] N. Khude, I. Stanciulescu, D. Melanz and D. Negrut, "Efficient parallel simulation of large flexible body systems with multiple contacts," *Journal of Computational and Nonlinear Dynamics,* vol. 8, no. 4, p. 041003, 2013.

[25] J. C. Wong, H. Kaymak, S. Brunner, and M. M. Koebel, "Mechanical properties of monolithic silica aerogels made from polyethoxydisiloxanes," *Microporous and Mesoporous Materials,* vol. 183, pp. 23-29, 2014.

[26] J. P. Hansen and I. R. McDonald, "Statistical mechanics of dense ionized matter. iv. density and charge fluctuations in a simple molten salt," *Physical Review A,* vol. 11, no. 6, p. 2111, 1975.

[27] J. N. Israelachvili, *Intermolecular and suface forces, revised third edition.* Academic press, 2011.

[28] E. P. Bellido and J. M. Seminario, "Molecular dynamics simulations of folding of supported graphene," *The Journal of Physical Chemistry C,* vol. 114, no. 51, pp. 22472-22477, 2010.

[29] D. J. Evans and B. L. Holian, "The nose-hoover thermostat," *The Journal of chemical physics,* vol. 83, no. 8, pp. 4069-4074, 1985.

[30] G. U. Gamboa, J. M. Vasquez-Perez, P. Calaminici, and A. M. Koster, "Influence of thermostats on the calculations of heat capacities from born-oppenheimer molecular dynamics simulations," *Wiley InterScience,* February 2010.

[31] G. J. Martyna, M. L. Klein, and M. Tuckerman, "Nose-hoover chains: the canonical ensemble via continuous dynamics," *The Journal of chemical physics,* vol. 97, no. 4, pp. 2635-2643, 1992.

[32] S. Nose, "Constant-temperature molecular dynamics," *J. Phys.: Condens. Matter,* vol. 2, pp. 15-19, 1990.

[33] A. P. Bowling, A. F. Palmer, and L. Wilhelm, "Contact and impact in the multibody dynamics of motor protein locomotion," *Langmuir,* vol. 25, no. 22, pp. 12974-12981, 2009.

[34] M. Haghshenas-Jaryani, B. Black, S. Ghaffari, J. Drake, A. Bowking and S. Mohanty, "Dynamics of microscopic objects in optical tweezers: experimental determination of underdamped regime and numerical simulation using multi-scale analysis," *Nonlinear Dynamics,* vol. 76, no. 2, pp. 1013-1030, 2014.
vspace2 mm

[35] M. Haghshenas-Jaryani, N. T. Tran, A. P. Bowling, J. A. Drake, and S. Mohanty, "Multiscale modeling and simulation of a microbead in an optical trapping process," in *ASME 2013 2nd Global Congress on NanoEngineering for Medicine and Biology.* American Society of Mechanical Engineers, 2013 pp. V001T05A003-V001T05A003.

[36] A. B. Rosenthal and S. H. Garofalini, "Structural role of zinc oxide in silica and soda-silica glasses," *Journal of the American Ceramic Society,* vol. 70, no. 11, pp. 821-826, 1987.

[37] M. G. Del Popolo and G. A. Voth, "On the structure and dynamics of ionic liquids," *The Journal of Physical Chemistry B,* vol. 108, no. 5, pp. 1744-1752, 2004.

[38] T. Megyes, S. Balint, E. Peter, T. Grosz, I. Bako, H. Keienke and M.-C. Bellissent-Funel, "Solution structure of nano3 in water: Diffraction and molecular dynamics simulation study," *The Journal of Physical Chemistry B,* vol. 113, no. 13, pp. 4045-4064, 2009.

[39] A. Lileev, Z. Filimonova, and A. Lyashchenko, "Dielectric permittivity and relaxation in aqueous solutions of alkali metal sulfates and nitrates in the temperature range 288-313 k," *Jounal of molecular liquids,* vol. 103, pp. 299-308, 2003.

BIOGRAPHICAL STATEMENT

Yatish Nagaraj was born in Bangalore, India in 1987. He received his Bachelor in Engineering (B.E.) degree in Mechanical Engineering from Visvesvaraya Technological University, Belguam, India in 2009. He was a lecturer in the department of mechanical engineering of East Point College of Engineering and Technology. He received his M.S. degree, also in the Mechanical Engineering from The University of Texas at Arlington in 2014. His current research interest is in the area of Robotics and Molecular Dynamics.